PERGAMON

International Journal of Multiphase Flow 25 (1999) 377–394

International Journal of Multiphase Flow

Gas–liquid two-phase flow in microchannels Part I: two-phase flow patterns

K.A. Triplett, S.M. Ghiaasiaan *, S.I. Abdel-Khalik, D.L. Sadowski

G. W. Woodruff School of Mechanical Engineering, Georgia Institute of Technology, Atlanta, GA 30332-0405, USA

Received 16 December 1997; received in revised form 18 August 1998

Abstract

Capillary gas–liquid two-phase flow occurs in increasingly more modern industrial applications. The existing relevant data are limited and are inconsistent with respect to the reported flow patterns and their transition boundaries. A systematic experimental investigation of two-phase flow patterns in microchannels was the objective of this study.

Using air and water, experiments were conducted in circular microchannels with 1.1 and 1.45 mm inner diameters, and in microchannels with semi-triangular (triangular with one corner smoothed) cross-sections with hydraulic diameters 1.09 and 1.49 mm. The gas and liquid superficial velocity ranges were 0.02–80 and 0.02–8 m/s, respectively. Overall, flow patterns and flow pattern maps using gas and liquid superficial velocities as coordinates, were similar for all the test sections. The discernible flow patterns were bubbly, churn, slug, slug–annular and annular. The obtained data were compared with existing experimental data. They were also compared with relevant flow regime transition models and correlations, generally with poor agreement.

Keywords: Microchannels; Two-phase flow; Flow patterns; Adiabatic flow; Circular channels; Non-circular channels

1. Introduction

Flow channels with hydraulic diameters of the order of, or smaller than, the Laplace constant,

$$\sqrt{\frac{\sigma}{g(\rho_L - \rho_G)}},$$

* Corresponding author. Fax: 001 404 894 3733; E-mail: seyed.ghiaasiaan@me.gatech.edu.

0301-9322/99/$ - see front matter
PII: S0301-9322(98)00054-8

(where σ represents the surface tension, $\boldsymbol{g}$ is the gravitational constant, and ρ_L and ρ_G are liquid and gas densities, respectively) are applied in compact heat exchangers, microelectronic cooling systems, research nuclear reactors, chemical processing, and small-sized refrigeration systems. Gas–liquid two-phase flow frequently occurs in many of these applications. Design and operation of systems that include gas–liquid two-phase flow in capillaries requires that capillary two-phase flow characteristics, including flow patterns and two-phase pressure drop, be known.

The objective of the investigation reported in this article was to systematically study the gas–liquid two-phase flow patterns, void fraction, and pressure drop in capillaries with circular cross-sections and capillaries representing the flow channels in rod bundles with small, triangular-pitched arrays. In the present (part I) article, two-phase flow patterns are addressed. In part II of this article (Triplett et al., 1999) void fraction and two-phase pressure drop will be discussed.

2. Background

Two-phase flow characteristics of capillaries are known to be significantly different from the characteristics of larger channels, and consequently the existing vast literature associated with the phenomenology of change-of-phase heat transfer and two-phase flow hydrodynamic processes generally do not apply to capillaries. The surface tension is predominant in capillaries and significantly reduces the slip velocity, and renders the flow characteristics independent of channel orientation with respect to gravity. Criteria for determining the maximum channel diameter for channel orientation—independent (or, equivalently, gravity-independent) flow have been proposed by Suo and Griffith (1964), Brauner (1990), Brauner and Moalem-Maron (1992), and Fukano and Kariyasaki (1993). Furthermore, since the channel diameters are about equal to or smaller than the Laplace length scale, the hydrodynamic interfacial processes that are governed by Taylor instability do not apply to capillaries. Taylor instability, however, controls many crucial interfacial processes in larger channels.

Previous studies generally confirm significant differences between capillaries and large channels, with respect to two-phase pressure drop (Inasaka et al., 1989; Lin et al., 1991; Fukano and Kariyasaki, 1993; Fouran and Bories, 1995), boiling heat transfer and critical heat flux (Inasaka et al., 1989; Peng and Wang, 1993), and two-phase flow patterns (Suo and Griffith, 1964; Oya, 1971, Barnea et al., 1983; Fukano and Kariyasaki, 1993; Galbiati and Andreini, 1994).

Suo and Griffith (1964) performed experiments in horizontal channels with 0.5 and 0.7 mm diameters, and could identify slug, slug–bubbly, and annular flow patterns. For transition from slug to slug–bubbly, they suggest:

$$Re\,We = 2.8 \times 10^5, \tag{1}$$

where

$$Re = \rho_L D U_B / 2\mu_L, \tag{2}$$

$$We = D\rho_L U_B^2/2\sigma, \tag{3}$$

$$U_B = 1.2(U_{LS} + U_{GS}). \tag{4}$$

In the above Eqs. *Re* and *We* represent Reynolds and Weber numbers, respectively, D is the channel diameter, U_{LS} and U_{GS} are liquid and gas superficial velocities, respectively, ρ_L and μ_L are the liquid density and viscosity, respectively, σ is the surface tension, and U_B is the velocity of the gas bubbles. No stratified flow occurred in the experiments of Suo and Griffith (1964), and subsequent studies have confirmed that, with gas and water-like liquids, stratified flow does not occur in channels with diameters smaller than about 1 mm (Damianides and Westwater, 1988; Fukano and Kariyasaki, 1993).

Transition from stratified to slug flow patterns is an important flow regime transition and has been studied extensively in the past. A widely used semi-analytical model, due to Taitel and Dukler (1976), is based on a Kelvin–Helmholtz instability criterion applied to a stable stratified flow. Barnea et al. (1983) argued that in microchannels the predominance of surface tension on gravitational force, and not the Kelvin–Hemholtz type instability, is responsible for flow regime transition from stratified to slug. Accordingly, the regime transition was shown to occur when the liquid depth, h_L found from the solution of one-dimensional steady-state stratified momentum equations satisfied:

$$D - h_L \leq \frac{\pi}{4}\left[\frac{\sigma}{\rho_G\left(1-\frac{\pi}{4}\right)}\right]^{1/2}. \tag{5}$$

Furthermore, when D is smaller than the right hand side of the above equation, the flow transition criterion is (Barnea et al., 1983):

$$h_L \geq \left(1-\frac{\pi}{4}\right)D. \tag{6}$$

The criterion of Barnea et al. well predicts flow patterns of air and water in channels several mm in diameter (Barnea et al., 1983; Fukano and Kariyasaki, 1993). For smaller channels, however, the criteria of Taitel and Dukler (1976) and Barnea et al., (1983) both appear to do poorly (Fukano and Kariyasaki, 1993; Damianides and Westwater, 1988). More recently, based on a linear stability analysis of stratified flow and based on the argument that neutral stability should consider a disturbance wavelength of the order of channel diameter, Brauner and Moalem-Maron (1992) derived the following criterion for the dominance of surface tension

$$E\ddot{o} = \frac{(2\pi)^2\sigma}{(\rho_L - \rho_G)D^2\boldsymbol{g}} > 1 \tag{7}$$

with *Eö* representing the Eotvös number.

Two-phase flow patterns in microchannels, including channels with diameters close to 1 mm, have been recently studied by several investigators. Damianides and Westwater (1988) could identify bubbly, plug, slug, dispersed, and annular flow patterns. Fukano and Kariyasaki

(1993) reported bubbly, intermittent, and annular regimes, and noted poor agreement with the flow regime map of Mandhane et al. (1974). Furthermore, among the semi-analytical flow regime transition models of Taitel and Dukler (1976) and Taitel et al. (1980), only the following relation for transition to dispersed bubbly flow agreed with their data.

$$U_{LS} + U_{GS} = 4.0 \left\{ \frac{D^{0.429} \left(\sigma/\rho_L\right)^{0.089}}{v_L^{0.072}} \left[\frac{g\left(\rho_L - \rho_G\right)}{\rho_L} \right]^{0.446} \right\} \tag{8}$$

where v_L represents the liquid kinematic viscosity. Galbiati and Andreini (1994) performed experiments in a 1 mm inner diameter channel using air and water and only observed slug and annular flow patterns. Barajas and Panton (1993) examined the effect of surface wettability on flow patterns in 1.6 mm-diameter horizontal microchannels. For partially wetting fluid–solid combinations (contact angles smaller than 90°) the flow patterns were insensitive to the contact angle and flow regime maps were similar except for the rivulet flow regime which occurred in tests with 61 and 74° contact angles and its domain expanded as the contact angle increased. With a partially non-wetting combination (contact angle = 106°), however, the rivulet flow pattern region was considerably wide, and in comparison with partially wetting experiments some of the flow regime transition lines were noticeably displaced.

3. Experiments

3.1. Apparatus

Fig. 1 is a schematic of the test apparatus, where important components are designated with Roman letters, and measurement instruments are assigned numbers. The test loop components and measurement instruments are listed in Table 1.

Water, deionized in a three part filtering system (not shown in Fig. 1), and fully degassed by boiling at atmospheric pressure, is introduced into the test loop, and flows towards the mixer E via the flowmeters 4 or 5. The upstream pressure of the water and consequently its flow rate, are stabilized by the rubber bladder I, itself maintained pressurized by the constant-pressure steel tank J. The flow rate of air, after flowing through the regulator A, the air dryer B, and air filter C, is measured in flowmeters 1 or 2, and it is subsequently introduced into the mixer E. The air–water mixture then flows through the test section F.

Details of a test section (test section a, to be described below) and its vicinity, and the mixer, are displayed in Fig. 2(a) and (b), respectively. The mixer, as noted, is a cross component through which the test section passes. In the mixing chamber, gas flows into the test section through two radial holes, which are 1.59 mm in diameter.

Four different test sections were used in the experiments. Test sections (a) and (b) were 1.097 and 1.447 mm-bore Pyrex circular channels (Ace Glass Pyrex Part No. 7740). Test sections (c) and (d), depicted in Fig. 3, which will be referred to as the semi-rectangular test sections, are utilized to examine flow patterns in non-circular channels with sharp corners, while providing for easy visual observation of flow patterns.

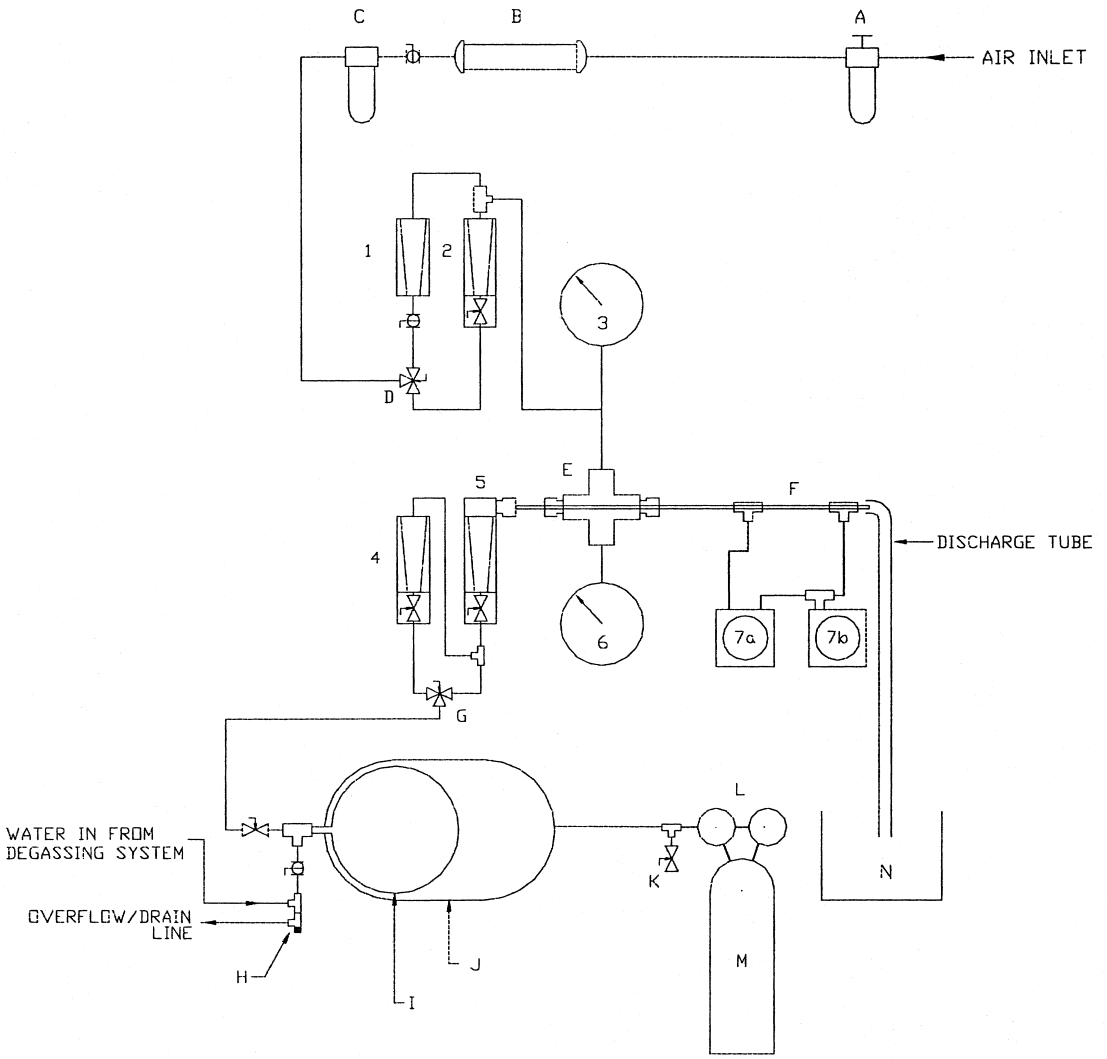

Fig. 1. Schematic of the test facility.

A 3.175 mm 60°, single flute countersink drill with a rounded tip was used to mill the triangular shaped channel along the length of the test section. An acrylic rod was utilized for the smaller semi-triangular channel (test section c), while a polycarbonated rod was used for the larger semi-triangular channel (test section d). Flat strips of acrylic were used to create a third side, or face, to the triangular shaped channel.

Prior to experiments, the test loop was carefully leak-tested by covering all the fittings with Buckeye Blue, a mixture of surfactants, while the highest liquid and air flow rates were imposed on the system. After all leaks were eliminated, the test loop and all the pressure taps were flushed with water to remove all trapped air pockets. Experiments were then performed

Table 1
Major components of the test apparatus

Label	Description	Manufacturer/model
A	Regulator	Speed Air/4Z029
B	Air dryer	Henry/7482
C	Air filter	Norgren/F39-200NOTA
D	Three-way valve	Whitey/B42XS4
E	Air/water mixing chamber	Cajun/B6CS
F	Experimental test section	In-house construction
G	Three-way valve	Whitey/B42XF2
H	Adjustable pressure relief valve	Watts/530
I	Rubber bladder containing degassed water	Teel/4P833A
J	Constant pressure steel tank	Teel/4P833A
K	Bleed valve	Hoke/151SG4 S
L	Regulator	National/3070
M	Nitrogen gas tank	Supplied by Air Products
N	Discharge container	Rubbermaid
1	Low volume rotameter glass and tantalum floats	Brooks/1110 tube no. R-2-15-AAA
2	High volume rotameter glass and tantalum floats	Brooks/135701F1AAA tube no. R-225-B
3	Air inlet pressure gauge	Heise/CC-99976
4	Low volume rotameter glass float	Brooks/1455EFA7BDB1A tube no. R-215-D
5	High volume rotameter glass float	Brooks/135501G1AAA tube no. R-615-B
6	Mixture pressure gauge	Crosby
7(a),(b)	Differential pressure transducers	Rosemount/1151DP5E22

by imposing a constant flow rate of degassed and deionized water at 25°C temperature, while varying the flow rate of air, also at 25°C.

The flow regimes in the test sections were identified visually with the aid of a strobe and a digital camera (Dalsa CA-D1), itself connected via a parallel port to a personal computer. The strobe was also connected to the computer's internal clock. The camera was always targeted at the test section centers. No systematic attempt was made to assess and eliminate the test section entrance effects on the flow regimes. However, the distance between the point pictured by the camera and the test section inlet was well over 100 channel diameters everywhere. Thus, although the possibility that the reported flow regimes are influenced by the test section entrance conditions exists, this influence may not be significant.

4. Results

4.1. Flow patterns

Fig. 4 displays representative photographs of the identified flow patterns in the 1.1 mm-inner diameter test section [test section (a)]. Five distinct flow patterns could be identified. Bubbly flow [Fig. 4 (a), (b)] was characterized by distinct and distorted (non-spherical) bubbles,

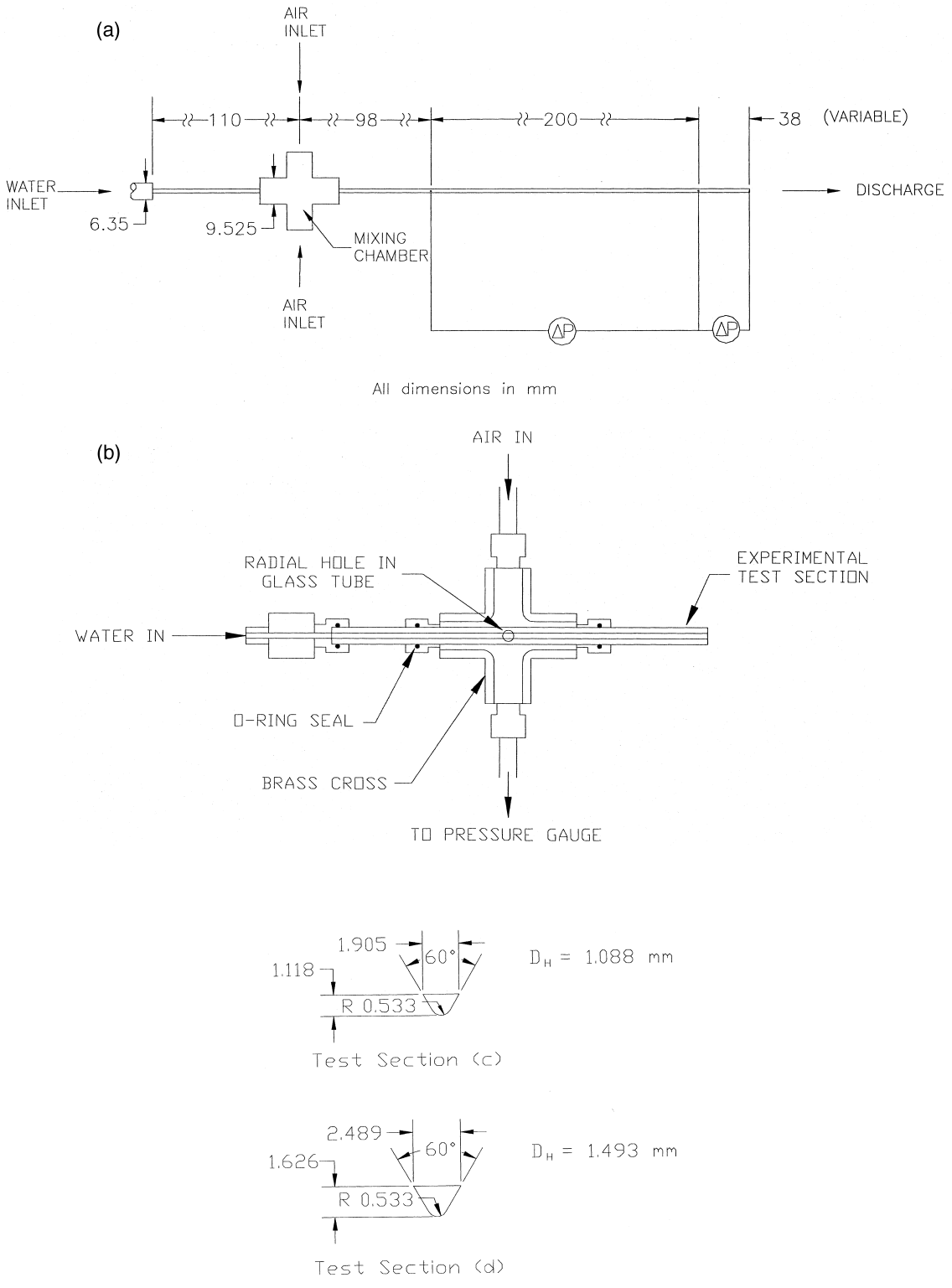

Fig. 3. Cross-sectional geometry of the test sections (c) and (d).

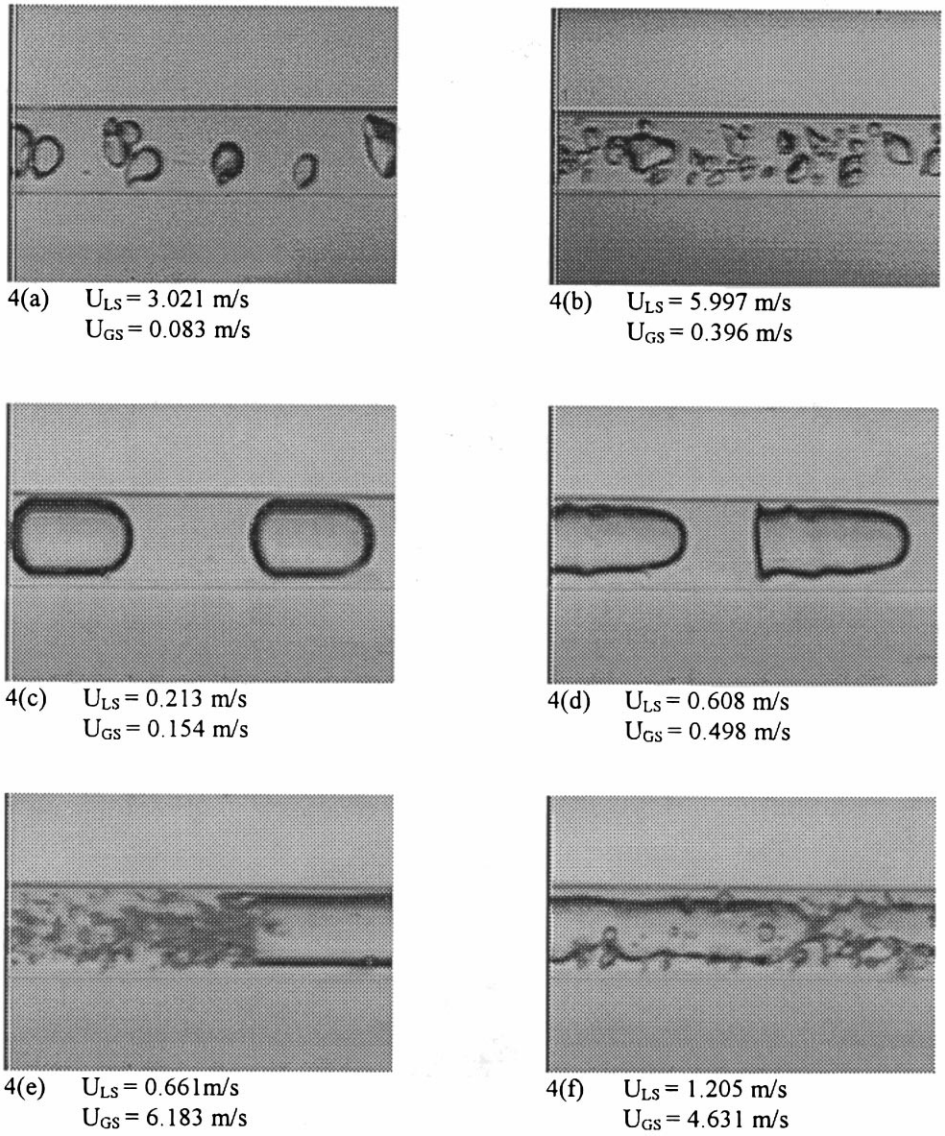

Fig. 4. Representative photographs of flow patterns in the 1.097 mm diameter circular test section [Test Section (a)]: (a), (b) bubbly; (c), (d) slug; (e), (f) churn; (g), (h) slug–annular; (i), (j) annular.

generally considerably smaller in diameter than the channel diameter. With increasing U_{GS} (which leads to increasing void fraction) the bubbles crowded near the channel top and eventually led to the development of the slug flow [Fig. 4 (c), (d)], characterized by elongated cylindrical bubbles. This flow pattern has been referred to by others as slug (Suo and Griffith, 1964), plug (Damianides and Westwater, 1988), and bubble-train (Thulasidas et al., 1997). Parameter changes leading to higher void fraction (e.g. increasing U_{GS} and/or decreasing U_{LS}) lead to longer bubbles and shorter liquid slugs. The bubbles, however, appear to effectively

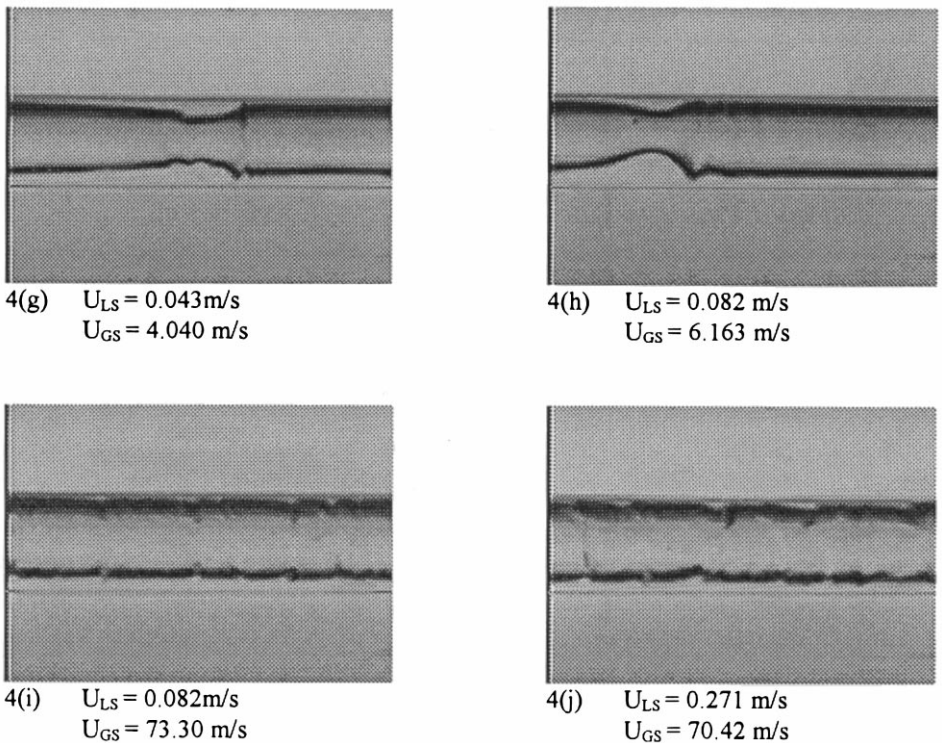

Fig. 4(g–j). *Continued.*

occupy most of the channel cross-section, with the liquid film at the bottom only slightly thicker than the liquid film at the top.

At high liquid superficial velocities U_{LS}, with increasing the mixture volumetric flux ($U_{LS}+U_{GS}$), churn flow was established. Two processes were assumed to characterize churn flow. In some cases the elongated bubbles in slug flow pattern became unstable near their trailing ends, leading to their disruption [Fig. 4(e)]. In others, flooding-type churning waves periodically disrupted an otherwise apparently wavy–annular flow [Fig. 4(f)]. The churn flow pattern defined here thus includes the aerated slug flow pattern, as the flow pattern represented by Fig. 4 (e) is sometimes referred to.

At relatively low liquid superficial velocities, increasing the mixture volumetric flux led to longer bubbles and shorter liquid slugs, eventually leading to the merging of elongated bubbles, and the development of the slug-annular flow pattern, represented by Fig. 4 (g), (h). In this flow pattern, long segments of the channel support an essentially wavy–annular flow, and are interrupted by large-amplitude solitary waves which do not grow sufficiently to block the flow path. With further increasing U_{GS}, these large amplitude solitary waves disappear and an annular flow pattern represented by Fig. 4 (i), (j) is obtained.

Representative photographs of the flow patterns in test section (c) (Fig. 3) are depicted in Fig. 5. Note that these pictures were taken while the camera was aimed perpendicular to the base of the cross-section of the test section, opposite to the smoothed corner. The identified

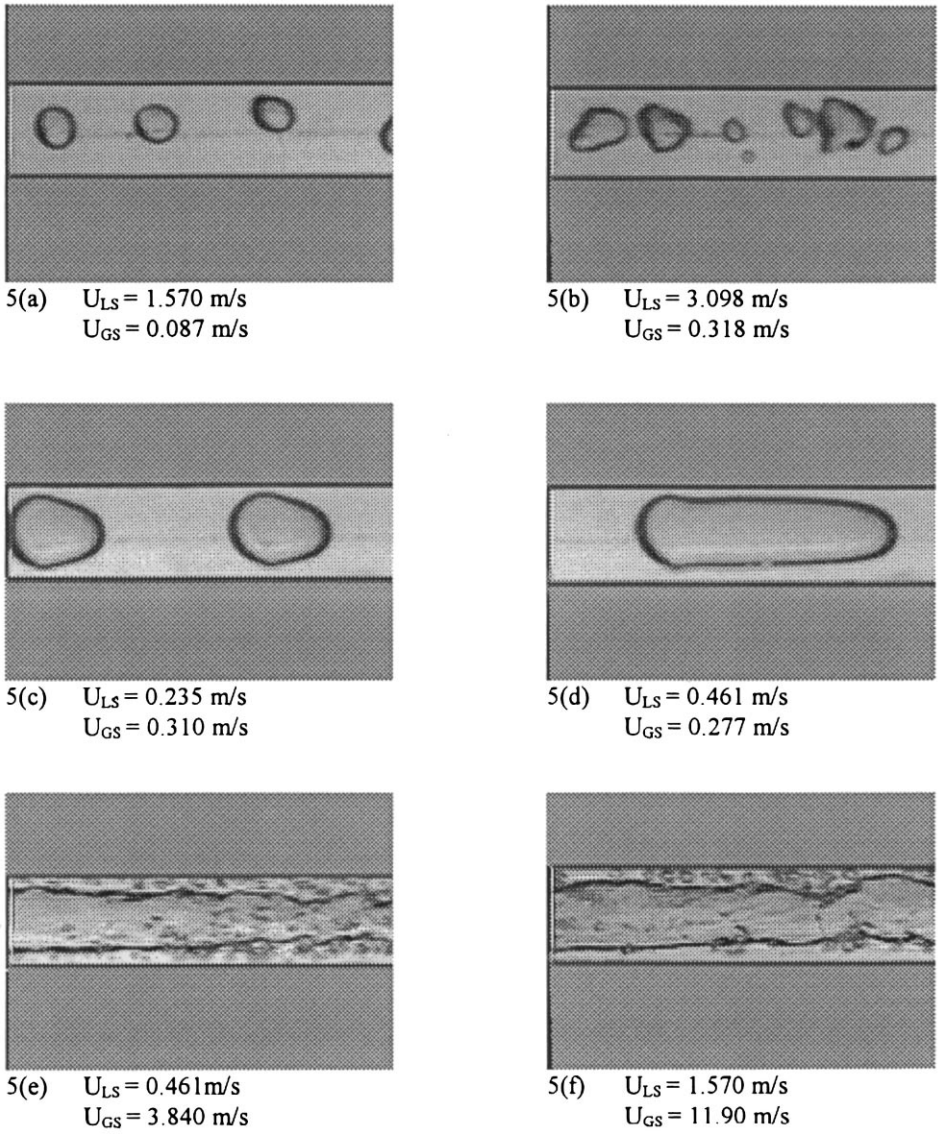

Fig. 5. Representative photographs of flow patterns in the 1.09 mm-hydraulic diameter semi-triangular test section [test section (c)]: (a), (b) bubbly; (c), (d) slug; (e), (f) churn; (g), (h) slug–annular; (i), (j) annular.

flow patterns were similar to those observed in circular test sections (bubbly, slug, churn, annular–slug, and annular). These flow patterns, furthermore, were similar to their corresponding flow patterns in the circular channels, at least with respect to their major morphological characteristics. Neither of the test sections supported stratified flow, confirming the predominance of surface tension.

The observed flow patterns and the flow pattern transition lines, are depicted in Fig. 6–9 for the test sections (a), (b), (c) and (d), respectively, in flow regime maps using U_{GS} and U_{LS} as coordinates. These flow patterns occurred at the center of the test sections. The depicted gas

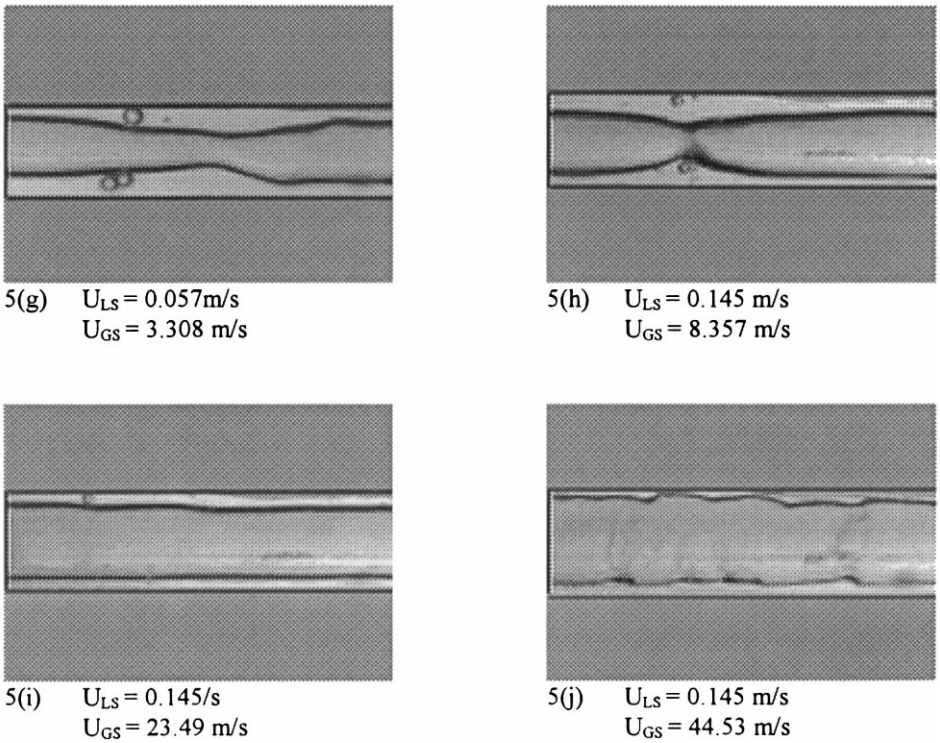

Fig. 5(g–j). *Continued.*

superficial velocities have been calculated based on the gas density itself calculated at a pressure equal to the average of the test section entrance and exit pressures. Overall, the flow regime maps for the circular and semi-triangular test sections were similar and were mostly covered by the slug and slug–annular flow patterns.

4.2. Comparison with available data and correlations

A comparison between the observed flow patterns and the flow regime map of Mandhane et al. (1974), which is representative of flow patterns in larger channels, showed poor agreement, confirming previously reported observations (Fukano and Kariyasaki, 1993).

The experimental flow patterns obtained in this study are compared with the correlation of Suo and Griffith (1964), Eqs. (1)-(4), and the mechanistic model of Taitel et al. (1980) for flow pattern transition line leading to dispersed bubbly flow pattern, Eq. (8), in Figs. 6–9. The expression suggested by Suo and Griffith significantly disagrees with the data. The model of Taitel et al. (1980) appears to satisfactorily predict the bubbly–slug transition line for all four test sections, and in particular for the circular test sections (Figs. 6 and 7). This observation is consistent with the results of Fukano and Kariyasaki (1993). Transition from dispersed bubbly to churn flow, however, appears to occur at a lower void fraction than 0.52.

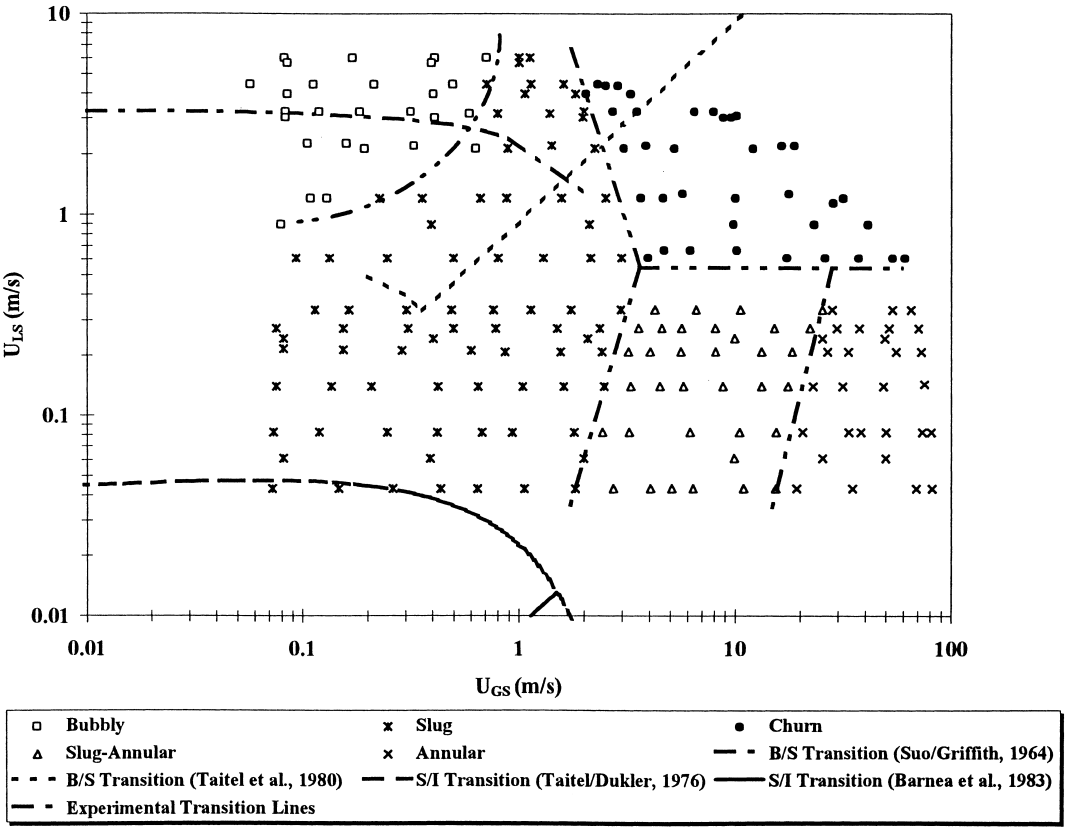

Fig. 6. Flow patterns and flow pattern transition lines for the 1.097 mm diameter circular test section [test section (a)].

The apparent agreement between the experimental bubbly–slug flow transition line and the model of Taitel et al. (1980) should be considered coincidental, however, since the assumptions leading to the derivation of the latter model do not apply to microchannels. The derivation of the latter model is based on the assumption that small bubbles generated due to turbulence can survive coalescence as long as they remain spherical, and as long as $\alpha \leq 0.52$. Two further assumptions leading to Eq. (8) are a locally–isotropic turbulent field and that the bubble diameter falls within the inertial zone of turbulent eddies (Hinze, 1955). It can be easily shown, however, that the assumption of locally–isotropic inertial eddies does not apply to the aforementioned microchannels.

Barnea et al. (1983) performed air–water experiments using test sections with diameters in the 4 to 12.3 mm range, and noted that the semi-analytical models of Taitel and Dukler (1976) (with a simple modification introduced into the slug–annular transition model) well-predicted all experimental two-phase flow regime transitions, except for the stratified-slug transition. Barnea et al. (1983) instead proposed a modified model, represented by Eqs. (5) and (6), for small channels. Predictions of the latter model are depicted in Figs. 6 and 7. No comparison is presented for semi-triangular channels since the model applies to circular channels only.

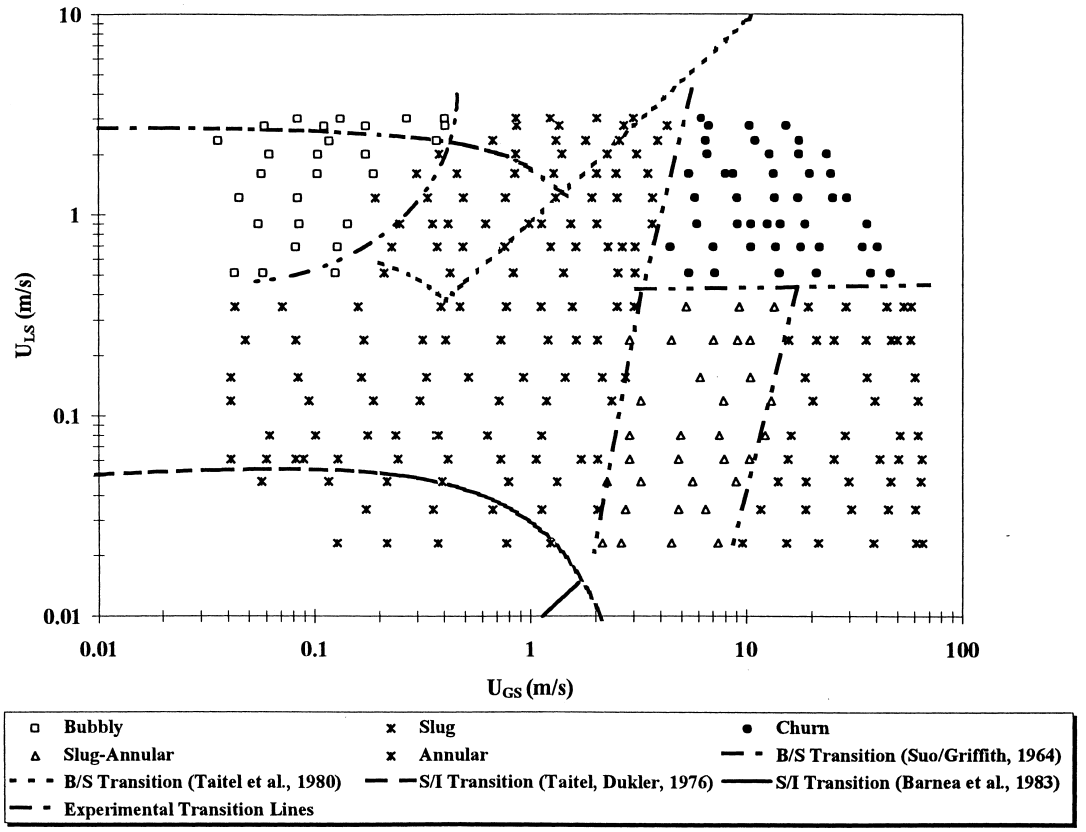

Fig. 7. Flow patterns and flow pattern transition lines for the 1.45 mm diameter circular test section [test section (b)].

As noted earlier, our experiments, in agreement with other similar experimental investigations, indicate that gas–liquid stratified flow does not occur in microchannels (Damianides and Westwater, 1988; Fukano and Kariyasaki, 1993). The precise conditions at which stratified flow becomes impossible are not known. Application of the criterion derived by Brauner and Moalem Maron (1993), Eq. (7), indicates that $Eö > 100$ for our experiments.

The observed flow patterns for the 1.1 mm diameter circular test section are compared with the experimental flow pattern transition lines of Damianides and Westwater (1988), representing their circular, 1 mm-inner diameter test section, in Fig. 10. The flow pattern names displayed on the figure represent the notation of Damianides and Westwater. The latter authors appear to have identified churn flow [Fig. 4 (e), (f)] as a dispersed flow pattern. The two data sets are in relative agreement with respect to slug and slug–annular (referred to as plug and slug, respectively, by Damianides and Westwater) flow patterns and the flow conditions leading to annular flow.

Fig. 11 displays the superficial velocity range, and the flow pattern transition lines, representing the experimental data of Fukano and Kariyasaki (1993) obtained with their circular, 1 mm-diameter test section, and compares them with the flow patterns observed with

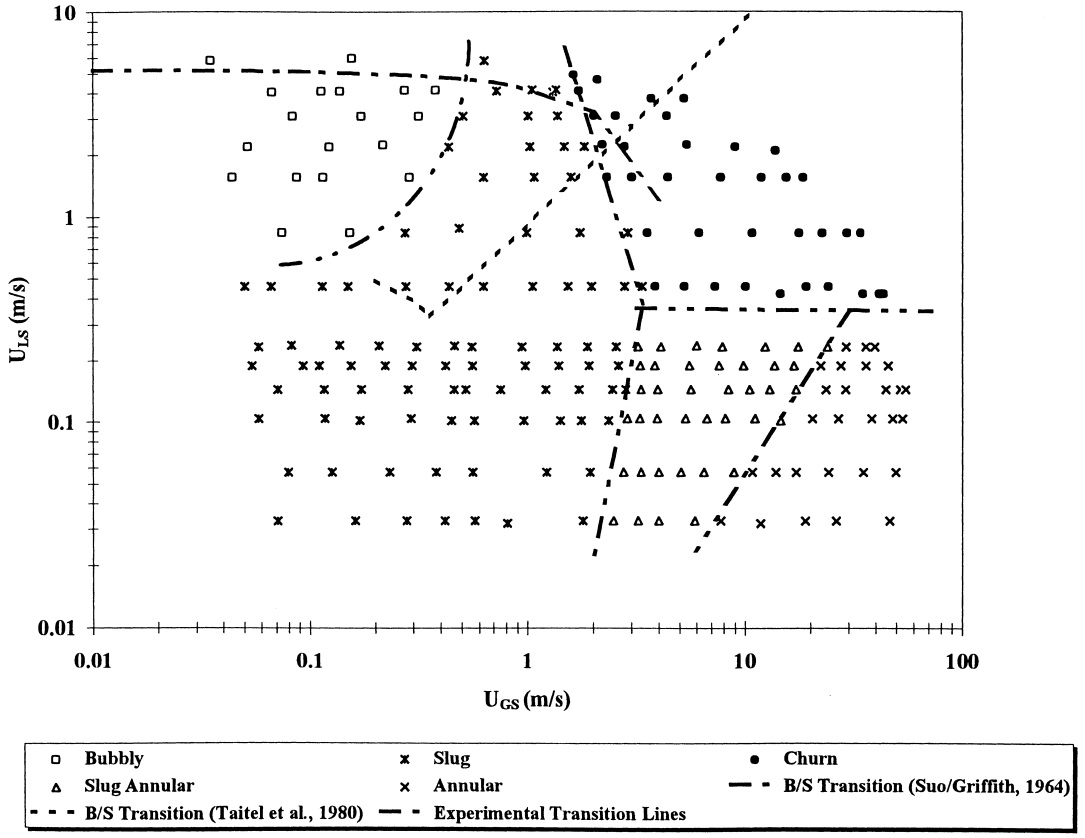

Fig. 8. Flow patterns and flow pattern transition lines for the 1.09 mm-hydraulic diameter semi-triangular test section [test section (c)].

our 1.1 mm-diameter circular test section. Fukano and Kariyasaki only distinguished three major flow patterns; bubbly, intermittent and annular. The two data sets are in relatively good agreement with respect to the slug (intermittent)—bubbly flow pattern transition line, which is relatively simple to identify experimentally due to the simplicity of the bubbly flow pattern's morphology. The intermittent flow pattern defined by Fukano and Kariyasaki (1993) evidently includes our slug, and most of our slug–annular flow patterns. The latter authors also appear to have included the churn flow regime zone [see Fig. 4 (e), (f)] in their intermittent and annular flow regime zones.

Barajas and Panton (1993) conducted experiments using air and water in horizontal 1.6 mm-diameter channels, using four different tube materials, which resulted in three partially-wetting combinations ($\theta = 34°$, $61°$, and $74°$, with θ representing the contact angle), and one partially-nonwetting ($\theta = 106°$) combination. With the partially wetting combinations, their flow regime maps were similar and had minor differences with the flow regime map of Damianides and Westwater (1988) for 1 mm-diameter channel. With $\theta = 34°$ (obtained with a Pyrex test section), however, they observed stratified–wavy flow in the $U_{GS} \lesssim 0.01$ m/s and 10 m/s $\lesssim U_{LS} \lesssim 100$ m/s range. With other test section materials this region of their flow regime map

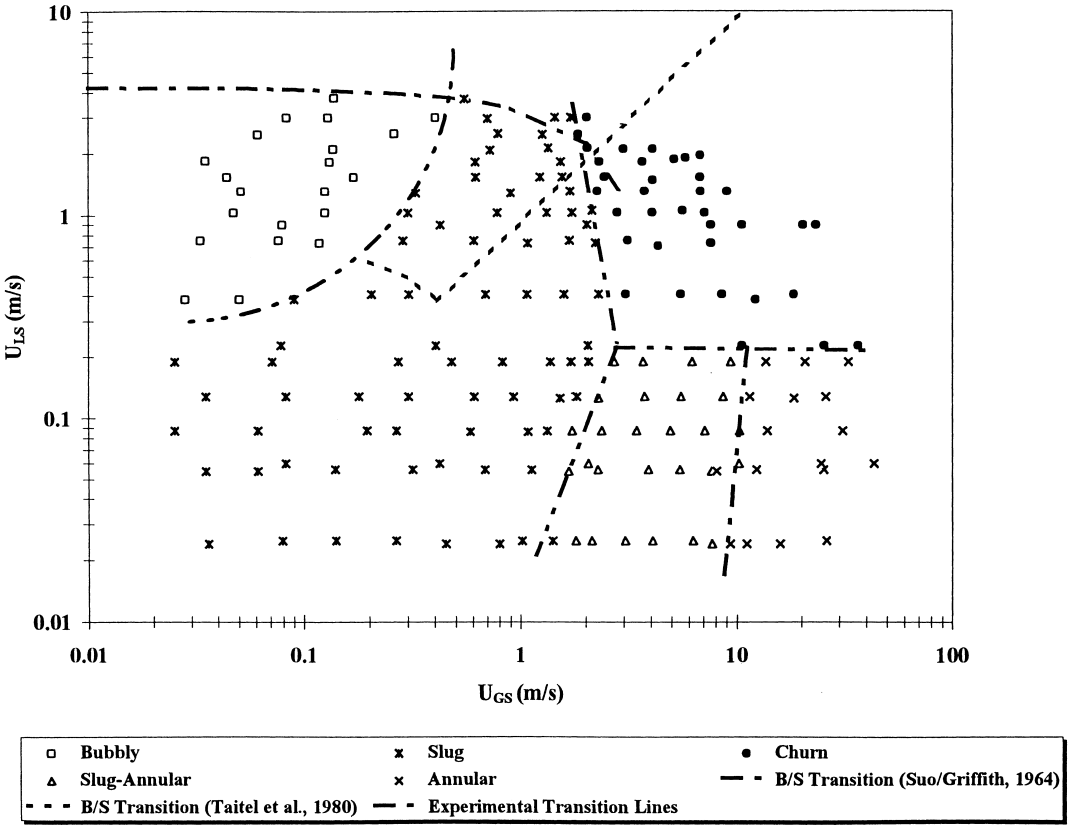

Fig. 9. Flow patterns and flow pattern transition lines for the 1.49 mm-hydraulic diameter semi-triangular test section [test section (d)].

was covered by the rivulet and multi-rivulet flow patterns. Our experiments did not cover the above range of superficial velocities. The rivulet and multi-rivulet regimes predominantly occurred at high U_{GS} (typically higher than 10 m/s) and low U_{LS} (typically less than 0.1 m/s), and its range of occurrence expanded as θ increased. Stratified–wavy and rivulet and multi-rivulet flow patterns have not been observed by Suo and Griffith (1964) or Fukano and Kariyasiaki (1993), and most importantly by Damianides and Westwater (1988) who used Pyrex test sections and whose experimental parameters clearly bracketed those of Barajas and Panton (1993). The aforementioned criterion of Brauner and Moalem-Maron (1992), Eq. (7), is well satisfied for all of the above experimental data. Based on material properties, in our experiments $\theta = 34^\circ$ for the Pyrex test sections a and b, 72° for the acrylic section c (Smedley, 1990), and about 78° for the polycarbonate test section d (Koh et al., 1995). All our experiments have thus used partially-wetting fluid–solid systems.

The experimental data obtained in this study, as noted, are in satisfactory overall agreement with similar experimental data of Damianides and Westwater (1988) and Fukano and Kariyasaki (1993), when inconsistencies associated with the identified flow patterns are removed. These experimental data, however, have all been obtained with air and water. Similar

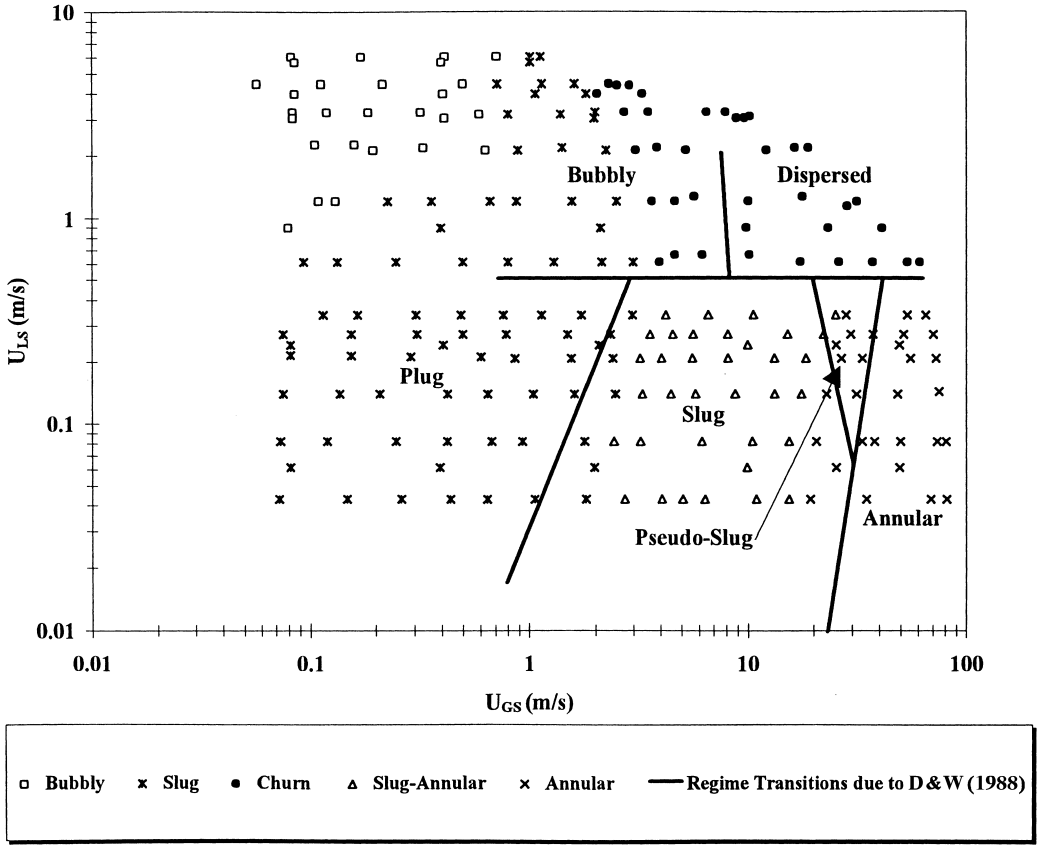

Fig. 10. Comparison between the experimental flow patterns obtained with test section (a) and the experimental flow regime transition lines of Damianides and Westwater (1988) representing their 1 mm-diameter circular test section.

experiments using other fluids are recommended in order to examine the effects of their properties on flow patterns. Measurement and correlation of void fraction, phasic velocities and frictional pressure drops are also needed.

5. Concluding remarks

Gas–liquid two-phase flow patterns, void fraction and pressure drop in long horizontal microchannels with circular and semi-triangular (triangular with one corner smoothed) cross-sections, were experimentally investigated. The test section hydraulic diameters were 1.1 and 1.45 mm for circular channels, and 1.09 and 1.49 mm for semi-triangular cross-section test sections, and the gas and liquid superficial velocity ranges were 0.02–80 m/s, and 0.02–8 m/s, respectively. Flow patterns are presented and discussed in this part. Void fraction and pressure drop are discussed in part II of this paper.

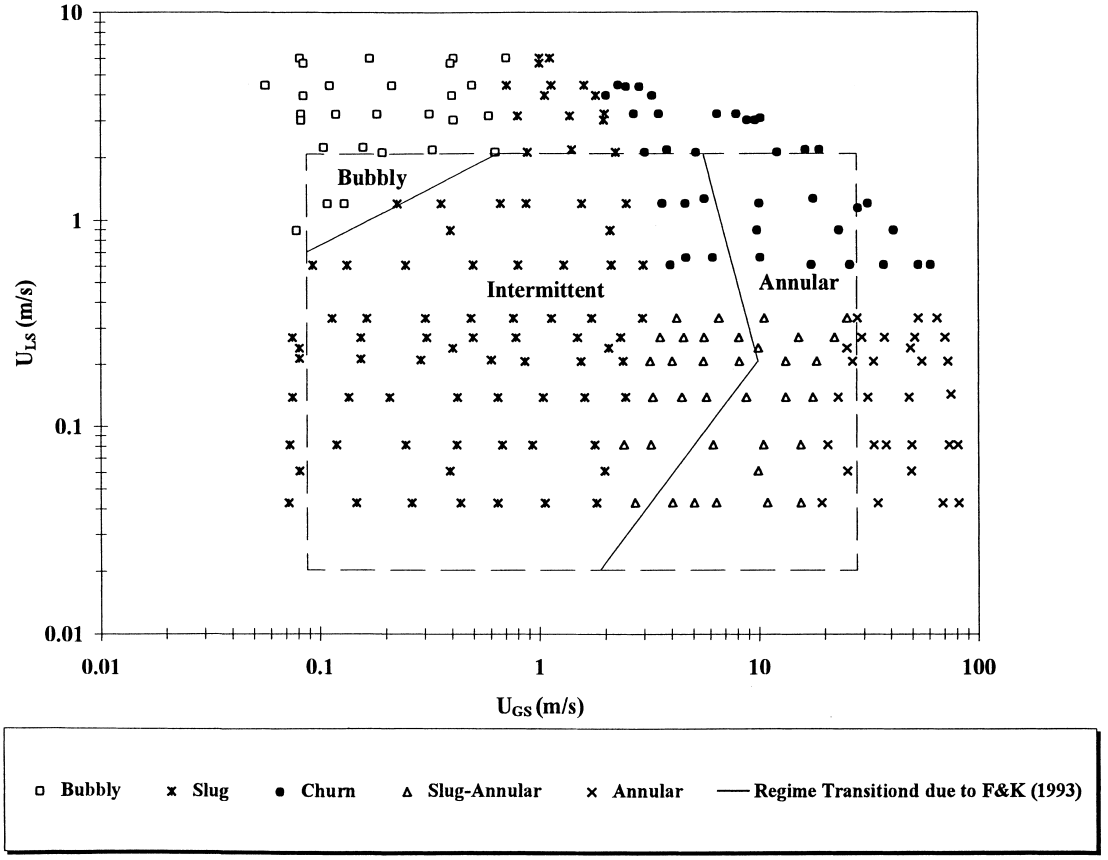

Fig. 11. Comparison between the experimental flow patterns with the flow patterns of Fukano and Kariyasaki (1993) representing their 1 mm-diameter circular test section.

Five major flow patterns could be distinguished in the experiments: bubbly, slug, churn, slug–annular and annular. These flow patterns occurred in all test sections and the flow pattern maps using gas and liquid superficial velocities as coordinates were similar overall.

The experimental data were compared with similar data of Suo and Griffith (1964), Damianides and Westwater (1988), and Fukano and Kariyasaki (1993), with good overall agreement with the latter two test series and with inconsistencies mainly attributable to confusion in the identification of flow patterns. Available relevant flow regime transition models were compared with data, with poor agreement.

References

Barajas, A.M., Panton, R.L., 1993. The effect of contact angle on two-phase flow in capillary tubes. Int. J. Multiphase Flow 19, 337–346.

Barnea, D., Luninski, Y., Taitel, Y., 1983. Flow in small diameter pipes. Can. J. Chem. Engng. 61, 617–620.

Brauner, N., 1990. The relation between two-phase flow under reduced gravity and earth experiments. Int. Commun. Heat Mass Transfer 17, 271–282.

Brauner, N., Moalem-Maron, D., 1992. Identification of the range of small diameter conduits, regarding two-phase flow pattern transitions. Int. Commun. Heat Mass Transfer 19, 29–39.

Damianides, C.A., Westwater, J.W., 1988. Two-phase flow patterns in a compact heat exchanger and in small tubes. In: Proc. Second UK National Conf. on Heat Transfer, Glasgow, 14–16 September. Mechanical Engineering Publications, London, pp. 1257–1268.

Fouran, M., Bories, S., 1995. Experimental study of air–water two-phase flow through a fracture (narrow channel). Int. J. Multiphase Flow 21, 621–637.

Fukano, T., Kariyasaki, A., 1993. Characteristics of gas–liquid two-phase flow in a capillary. Nucl. Engng. Des. 141, 59–68.

Galbiati, L., Andreini, P., 1994. Flow pattern transition for horizontal air–water flow in capillary tubes. A microgravity "equivalent system" simulation. Int. Commun. Heat Mass Transfer 21, 461–468.

Hinze, J.O., 1955. Fundamentals of the hydrodynamic mechanism of splitting in dispersion processes. AIChE J. 1, 289–295.

Inasaka, F., Nariai, H., Shimura, T., 1989. Pressure drops in subcooled flow boiling in narrow tubes. Heat Transfer Jap. Res. 18, 70–82.

Koh, S-K., Song, S-K., Choi, W-K., Jung, H-J., 1995. Improving wettability of polycarbonate and adhesion with aluminum by Ar^{+} ion irradiation. J. Mater. Res. 10, 2390–2394.

Lin, S., Kwok, C.C.K., Li, R-Y., Chen, Z-H., Chen, Z-Y., 1991. Local frictional pressure drop during vaporization of R-12 through capillary tubes. Int. J. Multiphase Flow 17, 95–102.

Mandhane, J.M., Gregory, G.A., Aziz, K., 1974. A flow pattern map for gas-liquid flow in horizontal pipes. Int. J. Multiphase Flow 1, 537–553.

Oya, T., 1971. Upward liquid flow in small tube into which air streams. Bull. JSME 14, 1320–1329.

Peng, X.F., Wang, B-X., 1993. Forced convection and flow boiling heat transfer for liquid flowing through microchannels. Int. J. Heat Mass Transfer 36, 3421–3427.

Smedley, G., 1990. Preliminary drop-tower experiments on liquid-interface geometry in partially filled containers at zero gravity. Exp. Fluids 8, 312–318.

Suo, M., Griffith, P., 1964. Two-phase flow in capillary tubes. J. Basic Engng. 86, 576–582.

Taitel, Y., Dukler, A.E., 1976. A model for predicting flow regime transition in horizontal and near horizontal gas liquid flow. AIChE J. 22, 47–55.

Taitel, Y., Bornea, D., Dukler, A.E., 1980. Modeling flow pattern transitions for steady upward gas–liquid flow in vertical tubes. AIChE J. 26, 345–354.

Thulasidas, T.C., Abraham, M.A., Cerro, R.L., 1997. Flow Patterns in liquid slugs during bubble-train flow inside capillaries. Chem. Engng. Sci. 52, 2947–2962.

Triplett, K.A., Ghiaasiaan, S.M., Abdel-Khalik, S.I., LeMouel, A., McCord, B.B., 1999. Gas–Liquid two-phase flow in microchannels. Part II: void fraction and pressure drop. Int. J. Multiphase Flow 25, 395–410.